Forcing term in single-phase and Shan-Chen-type multiphase lattice Boltzmann models

Haibo Huang,[1,2] Manfred Krafczyk,[1] and Xiyun Lu[2]
[1]*Institute for Computational Modeling in Civil Engineering, Technische Universität, D-38106 Braunschweig, Germany*
[2]*Department of Modern Mechanics, University of Science and Technology of China, Hefei, Anhui 230026, China*
(Received 29 April 2011; revised manuscript received 5 August 2011; published 25 October 2011)

Numerous schemes have been proposed to incorporate a bulk forcing term into the lattice Boltzmann equation. In this paper we present a simple and straightforward comparative analysis of five popular schemes [Shan and Chen, Phys. Rev. E **47**, 1815 (1993); Phys Rev Lett. **81**, 1618 (1998); He *et al.*, Phys. Rev. E **57**, R13 (1998); Guo *et al.*, Phys. Rev. E **65**, 046308 (2002); Kupershtokh *et al.*, Comput. Math. Appl. **58**, 965 (2009)] in which their differences and similarities are identified. From the analysis we classify the schemes into two groups; the behaviors of the schemes in each group are proven to be identical up to second order. Numerical test simulating the two-dimensional unsteady Taylor-Green vortex flow problem demonstrate that all five schemes are of comparable accuracy for single-phase flow. However, for two-phase flow the situation is different, which is demonstrated by incorporating these schemes into different Shan-Chen-type multiphase models. The forcing scheme in the original Shan-Chen (SC) multiphase model turns out to be inaccurate in terms of the resulting surface tension for different density ratios and relaxation times. In the numerical tests, a typical equation of state and interparticle interactions including next-nearest neighbors were incorporated into the SC model. Our results confirm that the surface-tension values obtained from the original SC lattice Boltzmann method (LBM) simulation depend on the value of the relaxation time τ. For $\tau < 0.7\Delta t$, the surface tension agree well with the analytical solutions. However, when $\tau > 0.7\Delta t$, the surface tension turns out to be systematically larger than the analytical one, exceeding it by more than a factor of 2 for $\tau = 2\Delta t$. In contrast, with the application of the scheme proposed by He *et al.*, the SC LBM produces very accurate surface tensions independent of the value of τ. We also found that the densities of the coexisting liquid and gas can be adjusted to match those at thermodynamic equilibrium if the particle interaction term includes next-nearest-neighbor contributions. The obtained results will be useful for further studies of two-phase flow with high density ratios using the SC LBM approach.

DOI: 10.1103/PhysRevE.84.046710 PACS number(s): 47.11.−j, 05.20.Dd, 68.03.Cd, 02.70.Ns

I. INTRODUCTION

Over the past decade, the lattice Boltzmann method (LBM), which is based on mesoscopic kinetic equations, has become a numerically robust and efficient technique for simulating both single-phase and multiphase fluids [1–4]. For both single-phase and multiphase flows, the correct treatment of the forcing term in the LBM is an important issue. Guo *et al.* [5] and Buick and Greated [6] discussed various schemes in the literature. In the course of the derivation of the Navier-Stokes (NS) equation from the lattice Boltzmann equation (LBE), Guo *et al.* [5] analyzed important properties as well as the accuracy of different forcing strategies. However, in the previous studies the connections between the forcing schemes of the Shan-Chen-type multiphase models [1] and Luo [7] were not investigated. Based on a straightforward theoretical analysis, we demonstrate that they are identical when neglecting terms of $O(\frac{\mathbf{F}^2\Delta t\tau}{\rho})$. Recently, Kupershtokh *et al.* [8] proposed the so-called exact difference method. After a simple analysis, we demonstrate that this forcing scheme is identical to the one used by Shan and Chen [1] and Luo [7] up to terms of $O(\frac{(\mathbf{F}\Delta t)^2}{\rho})$.

The present authors are unaware of previous studies investigating the connection between the forcing scheme proposed by He *et al.* [9] and that proposed by Ladd and Verberg [5,10]. The analysis given herein shows that the two schemes are identical at the macroscopic level when omitting terms of $O(u^3)$. These analytical results will be confirmed by simulations of the unsteady Taylor-Green vortex flow problem, which, due to the availability of an analytic solution, is a suitable benchmark to test the accuracy of numerical schemes in general and the various forcing schemes in particular.

For simulations of two-phase flows, the forcing-term strategy is of critical importance. Some popular LBM multiphase models, e.g., the color-gradient-based LBM [11–13] and the free-energy-based LBM [14], usually do not involve forcing terms explicitly. However, the popular models proposed by He *et al.* [4,15] and Shan and Chen [1] depend on accurate forcing strategies. Different discretization schemes for the forcing term in the model of He *et al.* [4,15] have been discussed by Wagner [16] and Kikkinides *et al.* [17] in detail. Kikkinides *et al.* [17] discovered that in order to make the model [15] thermodynamically consistent, the surface tension is limited to a very narrow range. In addition, they showed that only through a special discretization of the forcing term can thermodynamic consistency for the model of He *et al.* [15] be achieved [17].

The Shan-Chen (SC) model has been shown to lack thermodynamic consistency [18,19] and the surface tension in the model cannot be adjusted independently of the density ratio. However, in many applications this thermodynamic inconsistency is not of primary importance. Recently, Sbragaglia *et al.* [20] argued that surface tension can be adjusted for constant density ratios. The proposed method [20] extended the interparticle action up to next-nearest neighbors. Kupershtokh also proposed a similar strategy [8]. In contrast, to improve numerical stability, Yu and Fan [21] extended the SC model to a multiple-relaxation-time version. In this work we will focus exclusively on the SC Bhatnagar-Gross-Krook (BGK) model.

 ©2011 American Physical Society

In the SC model, by incorporating a forcing term into the corresponding LBE, the ideal-gas equation of state (EOS) in single-phase LBMs is substituted by a nonmonotonic EOS. Several researchers [3,22,23] have proposed a simple implementation strategy to incorporate different EOSs into the SC LBM to achieve high density ratios. Yuan and Schaefer [22] investigated the magnitude of spurious currents and the resulting coexistence curves for five different EOSs. However, the important issue of surface-tension variations in the SC LBM has not been discussed. This issue will also be addressed in this work.

In Ref. [18] the surface tension obtained from the SC model with $\tau = 0.6\Delta t$ is consistent with analytical solutions. However, the effect of varying τ on the results is not addressed. We will show that both the resulting density ratio and the surface tension strongly depend on τ when using the original SC model by carrying out simulations with different τ values for two typical EOSs. The numerical tests will be performed for both the original SC model and variants with a different forcing strategy. In addition, we will also investigate the midrange interaction in the SC model [20] involving a stencil exceeding nearest neighbors. The SC model in combination with the forcing strategy of He *et al.* [9] is found to generate a much more accurate surface tension than the original SC model.

In the following we first briefly review and analyze the five forcing schemes by conducting numerical tests to evaluate their accuracy for a single-phase flow problem. Then these schemes are incorporated into the SC model. The original SC model and the forcing-scheme models of He *et al.* [9] and Kupershtokh *et al.* [8] are compared in detail. In the comparison, the resulting surface tension and density ratios of a typical EOS will be discussed in detail.

II. LATTICE BOLTZMANN METHOD

In order to simplify the discussion, we focus on two-dimensional problems. It is expected that the results will be qualitatively identical for three-dimensional problems. The LBM can be derived from the BGK approximation of the Boltzmann equation [7]

$$\frac{\partial f}{\partial t} + \boldsymbol{\xi}\cdot\nabla f + \mathbf{F}\cdot\nabla_{\xi} f = -\frac{f - f^{\mathrm{eq}}}{\tau}, \tag{1}$$

where $f(\mathbf{x},\boldsymbol{\xi},t)$ is the single-particle distribution function in the phase space $(\mathbf{x},\boldsymbol{\xi})$, $f^{\mathrm{eq}}(\mathbf{x},\boldsymbol{\xi})$ is the Maxwell-Boltzmann distribution function, $\boldsymbol{\xi}$ is the microscopic velocity, $\mathbf{F}(\mathbf{x},t)$ is a body force, and τ is the relaxation time.

In the lattice BGK method, a distribution function f_i is introduced to implicitly represent all relevant properties of the fluid. This distribution function satisfies the following lattice Boltzmann equation [7]:

$$f_i(\mathbf{x}+\mathbf{e}_i\Delta t, t+\Delta t) = f_i(\mathbf{x},t) - \frac{\Delta t}{\tau}[f_i(\mathbf{x},t) - f_i^{\mathrm{eq}}(\mathbf{x},t)] + S_i(\mathbf{x},t), \tag{2}$$

where $f_i(\mathbf{x},t)$ is the density distribution function related to the discrete velocity direction i, τ is a relaxation time that is related to the kinematic viscosity by $\nu = c_s^2(\tau - 0.5\Delta t)$, and $S_i(\mathbf{x},t)$ is the source term added into the standard lattice Boltzmann equation. The equilibrium distribution function $f_i^{\mathrm{eq}}(\mathbf{x},t)$ can be calculated as [7]

$$f_i^{\mathrm{eq}}(\mathbf{x},t) = w_i\rho\left(1 + \frac{\mathbf{e}_i\cdot\mathbf{u}}{c_s^2} + \frac{(\mathbf{e}_i\cdot\mathbf{u})^2}{2c_s^4} - \frac{(\mathbf{u})^2}{2c_s^2}\right). \tag{3}$$

In Eqs. (2) and (3), $\mathbf{e}_i$ is the discrete velocity. For the D2Q9 model, they are given by [7]

$$[\mathbf{e}_0,\mathbf{e}_1,\mathbf{e}_2,\mathbf{e}_3,\mathbf{e}_4,\mathbf{e}_5,\mathbf{e}_6,\mathbf{e}_7,\mathbf{e}_8] = c\begin{bmatrix} 0 & 1 & 0 & -1 & 0 & 1 & -1 & -1 & 1 \\ 0 & 0 & 1 & 0 & -1 & 1 & 1 & -1 & -1 \end{bmatrix}.$$

In Eq. (3) we have $w_i = 4/9$ $(i = 0)$, $w_i = 1/9$ $(i = 1,2,3,4)$, $w_i = 1/36$ $(i = 5,6,7,8)$, and $c_s = \frac{c}{\sqrt{3}}$ for the D2Q9 model, where $c = \frac{\Delta x}{\Delta t}$ is the ratio of lattice spacing Δx and time step Δt. Here we define one lattice unit Δx as 1 l.u., one time step Δt as 1 t.s., and one mass unit as 1 m.u. In Eq. (3), ρ is the density of the fluid, which can be obtained from the discrete zeroth-order moment $\rho = \sum_i f_i$ and the fluid velocity $\mathbf{u} = \frac{1}{\rho}\sum_i f_i\mathbf{e}_i$ for $S_i = 0$.

III. FORCING TERM

To mimic the body force F_α in the incompressible Navier-Stokes equations

$$\begin{aligned} &\partial_t\rho + \partial_\alpha\rho u_\alpha = 0, \\ &\partial_t\rho u_\alpha + \rho u_\beta\partial_\beta u_\alpha = -\partial_\alpha p + \rho\nu\partial_\beta(\partial_\beta u_\alpha + \partial_\alpha u_\beta) + F_\alpha, \end{aligned} \tag{4}$$

usually an extra forcing term S_i is added to the LBE. Subscripts α and β indicate the coordinates x or y for the two-dimensional cases considered here. The Einstein summation convention is adopted. Numerous schemes have been proposed to include the forcing term in the LBM, five of which [1,5,7–10], labeled I–V, are discussed below.

A. Schemes to incorporate the body force

1. Scheme I

This scheme was proposed by Shan and Chen [1]. After the collision step, the momentum of the fluid particle is calculated as

$$\rho u_\alpha = \sum_i f_i e_{i\alpha}. \tag{5}$$

If a momentum $\mathbf{F}\tau$ acts on the fluid particle from internal or external body forces, the momentum of the fluid particle would reach a new equilibrium state with $\rho\mathbf{u}^{\mathrm{eq}}$ after $\Delta t = \tau$. From Newton's law of motion, the equilibrium velocity $\mathbf{u}^{\mathrm{eq}}$ is calculated by

$$u_\alpha^{\mathrm{eq}} = u_\alpha + \frac{\tau F_\alpha}{\rho}. \tag{6}$$

According to the SC model, this velocity should be substituted into Eq. (3) to calculate f_i^{eq}. In Eq. (6), the force acting on the fluid includes the interparticle force $\mathbf{F}_{\mathrm{int}}$ and external force $\mathbf{F}_{\mathrm{ext}}$. In this study $\mathbf{F}_{\mathrm{ext}} = 0$.

However, in the model the actual fluid velocity is not defined as $\mathbf{u}^{\mathrm{eq}}$, but as $\mathbf{u}^*$, which, according to Ref. [18], can be calculated by

$$u_\alpha^* = u_\alpha + \frac{F_\alpha \Delta t}{2\rho}. \tag{7}$$

Note that, in this scheme, the equilibrium velocity $\mathbf{u}^{\mathrm{eq}}$, which is plugged into Eq. (3), and the physical velocity $\mathbf{u}^*$ may not be identical. For schemes II–IV, the true fluid velocity $\mathbf{u}^*$ and the equilibrium velocity $\mathbf{u}^{\mathrm{eq}}$ are identical and $\mathbf{u}^* = \mathbf{u}^{\mathrm{eq}} = \mathbf{u}$.

2. Scheme II

Luo [7] described another scheme to incorporate the body force into the LBM that was derived from a nonideal-gas Boltzmann equation. Accordingly, the forcing term to be added into the LBE is [7]

$$S_i = w_i \left(\frac{1}{c_s^2}(e_{i\gamma} - u_\gamma) + \frac{1}{c_s^4} e_{i\alpha} u_\alpha e_{i\gamma} \right) F_\gamma \tag{8}$$

and the velocity is defined according to Eq. (5).

We also note the scaled forcing term introduced by Junk *et al.* [24]. In the scaled strategy, $S_i = \lambda S_i(\mathbf{x},t) + (1-\lambda) S_i(\mathbf{x} + \mathbf{e}_i \Delta t, t + \Delta t)$, where λ should satisfy $0 \leqslant \lambda \leqslant 1$. However, how to choose λ for a specific flow problem is not illustrated explicitly in Ref. [24]. In their practical tests, usually $\lambda = 1$ is adopted [24]. If $\lambda = 1$, it is identical to scheme II. Here we do not discuss the effect of the parameter λ and this scaled forcing strategy is not discussed in our study.

3. Scheme III

The idea of the scheme proposed by He *et al.* [9] is simple. On the left-hand side of Eq. (1) there is a force term $\mathbf{F} \cdot \nabla_{\boldsymbol{\xi}} f$. If f^{eq} is the leading part of f and the gradient of f^{eq} has a major contribution to the gradient of f, one finds [9] $\mathbf{F} \cdot \nabla_{\boldsymbol{\xi}} f \approx \mathbf{F} \cdot \nabla_{\boldsymbol{\xi}} f^{\mathrm{eq}} = -\mathbf{F} \cdot \frac{\boldsymbol{\xi} - \mathbf{u}}{c_s^2} f^{\mathrm{eq}}$. Considering discrete lattice effects, the corresponding formula for the forcing term according to Ref. [9] is

$$S_i = \left(1 - \frac{1}{2\tau}\right) \frac{1}{\rho c_s^2} F_\gamma (e_{i\gamma} - u_\gamma) f_i^{\mathrm{eq}} \tag{9}$$

and the velocity should be calculated as

$$u_\alpha = \sum_i f_i e_{i\alpha} + \frac{F_\alpha \Delta t}{2\rho}. \tag{10}$$

4. Scheme IV

Ladd and Verberg [10] proposed that the forcing term in the LBM should be expanded in a power series in the particle velocity, i.e.,

$$S_i = w_i \left(A + B_\gamma \frac{1}{c_s^2}(e_{i\gamma}) + C_{\alpha\gamma} \frac{1}{2c_s^4}\left(e_{i\alpha} e_{i\gamma} - c_s^2 \delta_{\alpha\gamma}\right) \right), \tag{11}$$

and the velocity should be defined by Eq. (10), where A, B_γ, and $C_{\alpha\gamma}$ are determined by a Chapman-Enskog expansion. Based on a careful derivation from the LBE to the NS equations, Guo *et al.* [5] suggested

$$S_i = \left(1 - \frac{1}{2\tau}\right) w_i \left(\frac{1}{c_s^2}(e_{i\gamma} - u_\gamma) + \frac{1}{c_s^4} e_{i\alpha} u_\alpha e_{i\gamma} \right) F_\gamma. \tag{12}$$

5. Scheme V

Recently, Kupershtokh *et al.* [8] proposed the exact difference method, which is derived directly from the Boltzmann equation. In this scheme, the source term in the LBE should be

$$S_i = f_i^{\mathrm{eq}}(\rho, \mathbf{u}^{\mathrm{eq}} + \Delta\mathbf{u}) - f_i^{\mathrm{eq}}(\rho, \mathbf{u}^{\mathrm{eq}}), \tag{13}$$

where

$$\Delta\mathbf{u} = \frac{F \Delta t}{\rho}. \tag{14}$$

In this scheme, the true fluid velocity $u_\alpha^* = \sum_i f_i e_{i\alpha} + \frac{F_\alpha \Delta t}{2\rho}$ and the equilibrium velocity $u_\alpha^{\mathrm{eq}} = \sum_i f_i e_{i\alpha}$ are not identical [8].

From the introduction above we can see that three terms may be modified by the presence of a body force: (i) the equilibrium velocity, (ii) the physical velocity, and (iii) the additional forcing term in the LBE. An overview of the five forcing schemes is shown in Table I. In schemes II–IV the true fluid velocity and the equilibrium velocity are identical, but for schemes I and V the velocities are slightly different. Scheme I is the only scheme that does not need an additional forcing term in the LBE.

TABLE I. Overview of the forcing schemes.

Scheme	Equilibrium velocity u_α^{eq}	Physical velocity u_α^*	Additional forcing term?
I	$\sum_i f_i e_{i\alpha} + \frac{\tau F_\alpha}{\rho}$	$\sum_i f_i e_{i\alpha} + \frac{F_\alpha \Delta t}{2\rho}$	no
II	$\sum_i f_i e_{i\alpha}$	$\sum_i f_i e_{i\alpha}$	yes
III	$\sum_i f_i e_{i\alpha} + \frac{F_\alpha \Delta t}{2\rho}$	$\sum_i f_i e_{i\alpha} + \frac{F_\alpha \Delta t}{2\rho}$	yes
IV	$\sum_i f_i e_{i\alpha} + \frac{F_\alpha \Delta t}{2\rho}$	$\sum_i f_i e_{i\alpha} + \frac{F_\alpha \Delta t}{2\rho}$	yes
V	$\sum_i f_i e_{i\alpha}$	$\sum_i f_i e_{i\alpha} + \frac{F_\alpha \Delta t}{2\rho}$	yes

We will prove that schemes I, II, and V are identical and schemes III and IV are identical with very minor differences. The former three and the latter two schemes are thus classified into two groups: A and B, respectively.

B. Theoretical analysis

We start by comparing the scheme in the original SC model (scheme I) to that of Luo [7] (scheme II). In the original SC model, the forcing term is incorporated by defining $\mathbf{u}^{\mathrm{eq}} = \mathbf{u} + \frac{1}{\rho}\tau\mathbf{F} = \frac{1}{\rho}(\sum_i f_i\mathbf{e}_i + \tau\mathbf{F})$ and in the collision step u^{eq} is substituted into f_i^{eq}. We note that the LBE can be rewritten as

$$\begin{aligned} f_i(\mathbf{x}+\mathbf{e}_i\Delta t, t+\Delta t) &= f_i(\mathbf{x},t) - \frac{\Delta t}{\tau}\left[f_i(\mathbf{x},t) - f_i^{\mathrm{eq}}(\mathbf{u}^{\mathrm{eq}})\right] \\ &= f_i(\mathbf{x},t) - \frac{\Delta t}{\tau}\left[f_i(\mathbf{x},t) - f_i^{\mathrm{eq}}(\mathbf{u})\right] \\ &\quad + \left(\frac{\Delta t}{\tau}\left[f_i^{\mathrm{eq}}(\mathbf{u}^{\mathrm{eq}}) - f_i^{\mathrm{eq}}(\mathbf{u})\right]\right), \end{aligned} \tag{15}$$

where the terms in large parentheses can be regarded as the source term in Eq. (2). Hence, in the SC model the explicit source term is

$$\begin{aligned} S_i &= \frac{\Delta t}{\tau}\left[f_i^{\mathrm{eq}}(\mathbf{u}^{\mathrm{eq}}) - f_i^{\mathrm{eq}}(\mathbf{u})\right] = \frac{\Delta t}{\tau}\left\{w_i\rho\left[1 + \frac{1}{c_s^2}e_{i\alpha}\left(u_\alpha + \frac{F_\alpha\tau}{\rho}\right) + \frac{1}{2c_s^4}e_{i\alpha}\left(u_\alpha + \frac{F_\alpha\tau}{\rho}\right)e_{i\beta}\left(u_\beta + \frac{F_\beta\tau}{\rho}\right)\right.\right. \\ &\quad \left.\left. - \frac{1}{2c_s^2}\left(u_\alpha + \frac{F_\alpha\tau}{\rho}\right)\left(u_\alpha + \frac{F_\alpha\tau}{\rho}\right)\right] - w_i\rho\left(1 + \frac{1}{c_s^2}e_{i\alpha}u_\alpha + \frac{1}{2c_s^4}e_{i\alpha}u_\alpha e_{i\beta}u_\beta - \frac{1}{2c_s^2}u_\alpha u_\alpha\right)\right\} \\ &= w_i\left(\frac{1}{c_s^2}(e_{i\alpha} - u_\alpha) + \frac{1}{c_s^4}e_{i\beta}u_\beta e_{i\alpha}\right)F_\alpha\Delta t + w_i\rho\frac{\Delta t}{\tau}\left[\frac{1}{2c_s^4}e_{i\alpha}e_{i\beta}\frac{F_\alpha F_\beta}{\rho^2}\tau^2 - \frac{1}{2c_s^2}\left(\frac{F_\alpha\tau}{\rho}\right)^2\right]. \end{aligned} \tag{16}$$

If terms of $O[\frac{\Delta t}{\tau}(\frac{F_\alpha F_\beta\tau^2}{\rho})]$ are neglected, scheme I is identical to scheme II [7]. We note that through expanding the distribution function in the Boltzmann equation on the basis of the Hermite orthogonal polynomials in velocity space, recently Shan *et al.* [25] derived a correction of $f_i^{\mathrm{eq}}(\mathbf{u}^{\mathrm{eq}})$. According to their study [25], in order to obtain second-order accuracy, the corrected $f_i^{\mathrm{eq}}(\mathbf{u}^{\mathrm{eq}})'$ should be

$$f_i^{\mathrm{eq}}(\mathbf{u}^{\mathrm{eq}}) - w_i\rho\frac{\Delta t}{\tau}\left[\frac{1}{2c_s^4}e_{i\alpha}e_{i\beta}\frac{F_\alpha F_\beta}{\rho^2}\tau^2 - \frac{1}{2c_s^2}\left(\frac{F_\alpha\tau}{\rho}\right)^2\right].$$

We observe that this correction is consistent with our present simple analysis because with this correction, the terms $O[\frac{\Delta t}{\tau}(\frac{F_\alpha F_\beta\tau^2}{\rho})]$ in Eq. (16) can be canceled.

In our numerical simulations presented below we found that the terms $O[\frac{\Delta t}{\tau}(\frac{F_\alpha F_\beta\tau^2}{\rho})]$ have a very minor effect on single-phase flow. However, in the following SC multiphase flow simulations, the terms $O[\frac{\Delta t}{\tau}(\frac{F_\alpha F_\beta\tau^2}{\rho})]$ are found to be of significant importance. Starting from $\sum_i S_i e_{i\alpha}e_{i\beta} = u_\alpha F_\beta + u_\beta F_\alpha + \frac{\Delta t}{\tau}(F_\alpha F_\beta\frac{\tau^2}{\rho})$, through a Chapman-Enskog expansion one can readily see the resulting NS equations with an extra body force of $O[\nabla\cdot\frac{\Delta t}{\tau}(F_\alpha F_\beta\frac{\tau^2}{\rho})]$ on the right-hand side (rhs) of the equations. In other words, what the original SC multiphase model really mimics is Eq. (4) with an extra complex nonlinear force term on the rhs.

We continue with the comparison of schemes V [8] and II [7]. In scheme V the source term is given by

$$\begin{aligned} S_i &= f_i^{\mathrm{eq}}(\rho,\mathbf{u}+\Delta\mathbf{u}) - f_i^{\mathrm{eq}}(\rho,\mathbf{u}) = w_i\rho\left[1 + \frac{1}{c_s^2}e_{i\alpha}\left(u_\alpha + \frac{F_\alpha\Delta t}{\rho}\right) + \frac{1}{2c_s^4}e_{i\alpha}\left(u_\alpha + \frac{F_\alpha\Delta t}{\rho}\right)e_{i\beta}\left(u_\beta + \frac{F_\beta\Delta t}{\rho}\right)\right. \\ &\quad \left. - \frac{1}{2c_s^2}\left(u_\alpha + \frac{F_\alpha\Delta t}{\rho}\right)\left(u_\alpha + \frac{F_\alpha\Delta t}{\rho}\right) - w_i\rho\left(1 + \frac{1}{c_s^2}e_{i\alpha}u_\alpha + \frac{1}{2c_s^4}e_{i\alpha}u_\alpha e_{i\beta}u_\beta - \frac{1}{2c_s^2}u_\alpha u_\alpha\right)\right] \\ &= w_i\left(\frac{1}{c_s^2}(e_{i\alpha} - u_\alpha) + \frac{1}{c_s^4}e_{i\beta}u_\beta e_{i\alpha}\right)F_\alpha\Delta t + w_i\rho\left[\frac{1}{2c_s^4}e_{i\alpha}e_{i\beta}\frac{F_\alpha F_\beta}{\rho^2}\Delta t^2 - \frac{1}{2c_s^2}\left(\frac{F_\alpha\Delta t}{\rho}\right)^2\right]. \end{aligned} \tag{17}$$

Similar to the case of Eq. (16), if we omit terms of $O(\frac{F_\alpha F_\beta\Delta t^2}{\rho})$, we observe that this formula is identical to the one proposed in the study of Luo [7]. Thus, for this scheme we encounter the same problem as the SC model analyzed above, i.e., it involves an extra nonlinear force in the NS equations. Hence we proved that schemes I, II, and V are identical if terms of $O(\frac{F_\alpha F_\beta\Delta t^2}{\rho})$ are omitted in schemes I and V.

Next we compare schemes III [9] and IV [5,10] in group B. In scheme III [9] the source term is given as

$$\begin{aligned} S_i &= \left(1-\frac{1}{2\tau}\right)\frac{1}{\rho c_s^2}F_\gamma(e_{i\gamma}-u_\gamma)f_i^{\mathrm{eq}} = \left(1-\frac{1}{2\tau}\right)\frac{1}{\rho c_s^2}F_\gamma(e_{i\gamma}-u_\gamma)w_i\rho\left(1+\frac{1}{c_s^2}e_{i\alpha}u_\alpha+\frac{1}{2c_s^4}e_{i\alpha}u_\alpha e_{i\beta}u_\beta-\frac{1}{2c_s^2}u_\alpha u_\alpha\right)\\ &= \left(1-\frac{1}{2\tau}\right)w_i\left(\frac{1}{c_s^2}(e_{i\gamma}-u_\gamma)+\frac{1}{c_s^4}e_{i\alpha}u_\alpha e_{i\gamma}\right)F_\gamma\\ &\quad+\left[\left(1-\frac{1}{2\tau}\right)w_i\left(-\frac{1}{c_s^4}e_{i\alpha}u_\alpha F_\gamma u_\gamma+\frac{1}{2c_s^6}e_{i\alpha}u_\alpha e_{i\beta}u_\beta F_\gamma(e_{i\gamma}-u_\gamma)-\frac{1}{2c_s^4}u_\alpha u_\alpha F_\gamma(e_{i\gamma}-u_\gamma)\right)\right]. \end{aligned} \tag{18}$$

In comparison to the schemes of Ladd and Verberg [10] and Guo *et al.* [5], i.e., Eq. (12), Eq. (18) yields extra terms S_i'. Omitting terms of $O(u^3)$, we find that the extra terms are

$$\begin{aligned} S_i' &= \left(1-\frac{1}{2\tau}\right)w_i\left(-\frac{1}{c_s^4}e_{i\alpha}u_\alpha F_\gamma u_\gamma+\frac{1}{2c_s^6}e_{i\alpha}u_\alpha e_{i\beta}u_\beta F_\gamma e_{i\gamma}\right.\\ &\quad\left.-\frac{1}{2c_s^4}u_\alpha u_\alpha F_\gamma e_{i\gamma}\right). \end{aligned} \tag{19}$$

By means of simple algebra, we find that $\sum_i S_i' = 0$, $\sum_i S_i' e_{i\kappa} = 0$, and $\sum_i S_i' e_{i\kappa}e_{i\delta} = 0$.

For the derivation of the NS equations from the LBE, only the zeroth- to second-order momenta of S_i are used. The S_i in Eq. (18) satisfies $\sum_i S_i = 0$, $\sum_i S_i e_{i\kappa} = (1-\frac{1}{2\tau})F_\kappa$, and $\sum_i S_i e_{i\kappa}e_{i\delta} = (1-\frac{1}{2\tau})(u_\kappa F_\delta + u_\delta F_\kappa)$, which can be used to derive NS equations correctly [5]. Hence the extra terms S_i' in scheme III do not affect the derivation. In other words, if terms of $O(u^3)$ are neglected, scheme III and IV are identical. As a preliminary conclusion, we proved that the schemes proposed by Luo [7], Kupershtokh *et al.* [8], and Shan and Chen [1] are identical when terms of $O(\frac{F_\alpha F_\beta \Delta t^2}{\rho})$ are omitted and the schemes proposed by He *et al.* [9], Guo *et al.* [5], and Ladd and Verberg [10] are identical when omitting terms of $O(u^3)$.

C. Numerical analysis for single-phase flow

We now validate these conclusions by simulating the unsteady Taylor-Green vortex flow. The analytical solutions for horizontal velocity u_a, vertical velocity v_a, and pressure are [5]

$$\begin{aligned} u_a &= -u_0\cos(k_1x)\sin(k_2y)e^{-\nu(k_1^2+k_2^2)t},\\ v_a &= u_0\frac{k_1}{k_2}\sin(k_1x)\cos(k_2y)e^{-\nu(k_1^2+k_2^2)t},\\ p &= p_0-\frac{G}{4}\left(\cos(2k_1x)+\frac{k1^2}{k2}\cos(2k_2y)\right)e^{-2\nu(k_1^2+k_2^2)t}, \end{aligned} \tag{20}$$

where k_1 and k_2 are the wave numbers in the x and y directions, respectively, which are fixed to unity in our simulations. The arbitrary pressure constant is set equal to $p_0 = 1.0$. The physical domain of our simulations is $x,y \in [-\pi,\pi]$.

In our simulations, the body force is a function of not only spatial position but also time, $F_x = -\rho k_1\frac{G}{2}\sin(2k_1x)e^{-2\nu(k_1^2+k_2^2)t}$ and $F_y = -\rho k_1^2\frac{G}{2k_2}\sin(2k_2y)e^{-2\nu(k_1^2+k_2^2)t}$, respectively, where $G = u_0^2$ represents the force magnitude and ν is the kinematic viscosity. A uniform mesh consisting of 128×128 grid nodes is used, which means $\Delta x = \frac{2\pi}{128}$. Periodic boundary conditions are applied in both directions. We note that $\nu = \frac{1}{3}\frac{\Delta x^2}{\Delta t}(\frac{\tau}{\Delta t}-0.5)$ and $\nu = 0.005$ is fixed in our simulations. For $\tau = 0.9\Delta t$, Δt in the simulation is about 0.06424. The flow is initialized by the analytical velocity and pressure (density) at $t = 0$. To eliminate the compressibility effect, u_0 is set equal to 0.001 l.u./t.s., which is small in our simulations. In our code, all the forcing schemes are implemented as follows: (i) streaming; (ii) compute density, equilibrium velocity, and real fluid velocity; (iii) compute forces; (iv) collision; (v) go back to (i).

We define the error of the velocity field as

$$E(t) = \sqrt{\frac{\sum\{[u(t)-u_a(t)]^2+[v(t)-v_a(t)]^2\}}{\sum[u_a(t)^2+v_a(t)^2]}}, \tag{21}$$

where the summation is over all grid nodes. We note that there seems to be a typographical error in the error definition [Eq. (29)] in Ref. [5] because, according this definition, $E(t)$ is found to be a constant in the simulation equal to $\sqrt{2}$.

From Fig. 1 we can see that when body force is not applied, the error decreases steadily with time. However, when body force is applied, the error decreases in an oscillatory way. From Figs. 1(b)–1(d) we can see that in the simulations with $\tau = 1.0\Delta t, 1.5\Delta t, 0.7\Delta t$, the error curves collapse onto a single curve. It is difficult to distinguish one from the others. All error curves decrease from 1.2% to 0.3% when time increases from $t = 0$ to 150. The error for these five schemes are almost identical. Although some study intended to exaggerate the difference between different schemes [5] by checking the error differences, the small difference between different schemes is beyond any practical significance. Hence, for single-phase flow, the five schemes result in almost identical accuracy.

IV. INTERPARTICLE FORCES IN THE SC MULTIPHASE LBM

In the original SC model, the interparticle force is defined as [2]

$$\mathbf{F}_{\mathrm{int}}(\mathbf{x},t) = -g\psi(\mathbf{x},t)\sum_i w_i\psi(\mathbf{x}+\mathbf{e}_i\Delta t,t)\mathbf{e}_i, \tag{22}$$

where g is a parameter that controls the strength of the interparticle force and ψ is a mean-field potential. In Ref. [1], $\psi(\rho) = \rho_0[1-\exp(-\rho/\rho_0)]$, where ρ_0 is a constant. Here the interaction is applied only to nearest neighbors. This interparticle force is subsequently referred to as interparticle-force model A.

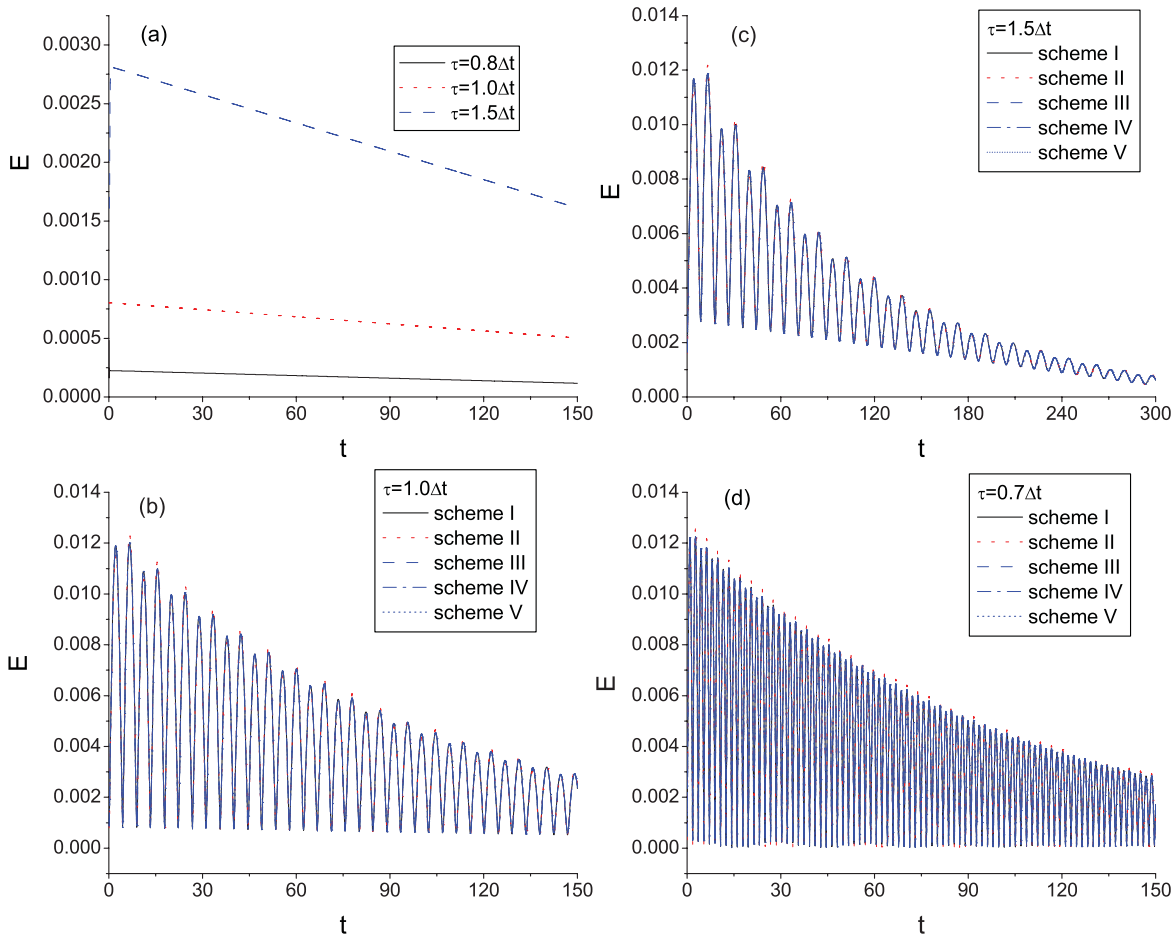

FIG. 1. (Color online) Error of the velocity field (a) when there is no body force applied and (b)–(d) as a function of the nondimensional time t for (b) $\tau = 1.0\Delta t$, (c) $\tau = 1.5\Delta t$, and (d) $\tau = 0.7\Delta t$, when body force is applied.

If interactions with next-nearest neighbors are also involved in the force computation, the value of the surface tension may be adjusted without changing the density ratio [20]. This interparticle force is defined as [20]

$$\mathbf{F}_{\text{int}}(\mathbf{x},t) = -\psi(\mathbf{x},t)\sum_i w_i[g_1\psi(\mathbf{x}+\mathbf{e}_i\Delta t,t) + g_2\psi(\mathbf{x}+2\mathbf{e}_i\Delta t,t)]\mathbf{e}_i, \tag{23}$$

where g_1 and g_2 are parameters that control the interactions with the nearest and next-nearest neighbors, respectively. It is referred to as interparticle-force model B.

For interparticle-force model A [Eq. (22)], one finds from the Taylor expansion as described in Appendix A in Ref. [19]

$$\begin{aligned} F_\alpha &= -g\psi\sum_i w_i\psi(\mathbf{x}+e_{i\alpha}\Delta t)e_{i\alpha} \\ &= -g\psi\Bigg(\sum_i w_i e_{i\alpha}\psi + \Delta t\sum_i w_i e_{i\alpha}e_{i\beta}\partial_\beta\psi \\ &\quad + \frac{1}{2}\Delta t^2\sum_i w_i e_{i\alpha}e_{i\beta}e_{i\gamma}\partial_\beta\partial_\gamma\psi \\ &\quad + \frac{1}{6}\Delta t^3\sum_i w_i e_{i\alpha}e_{i\beta}e_{i\gamma}e_{i\delta}\partial_\beta\partial_\gamma\partial_\delta\psi\Bigg) + \cdots \\ &\approx -\frac{g}{2}\Delta t c_s^2\partial_\alpha\psi^2 - \frac{g}{2}\Delta t^3 c_s^4\psi(\partial_\alpha\nabla^2\psi). \end{aligned} \tag{24}$$

The interparticle force can be translated into an excess pressure with respect to that of the ideal gas by

$$-\partial_\alpha p_{\alpha\beta} + \partial_\beta(c_s^2\rho) = F_\beta. \tag{25}$$

Then the total pressure tensor can be obtained as follows:

$$\begin{aligned} p_{\alpha\beta} &= \left[c_s^2\rho + \tfrac{1}{2}gc_s^2\psi^2 + \tfrac{1}{2}gc_s^4\left(\psi\nabla^2\psi + \tfrac{1}{2}|\nabla\psi|^2\right)\right]\delta_{\alpha\beta} \\ &\quad -\tfrac{1}{2}gc_s^4\partial_\alpha\psi\partial_\beta\psi. \end{aligned} \tag{26}$$

Compared with the well-known form of the pressure tensor [26] $p_{\alpha\beta} = [p - \kappa\rho\nabla^2\rho - \frac{1}{2}\kappa(\nabla\rho)^2]\delta_{\alpha\beta} + \kappa\partial_\alpha\rho\partial_\beta\rho$, we know that if $\kappa = -\frac{1}{2}gc_s^4$ and $\psi \propto \rho$, the pressure tensor is consistent with this well-known form. Hence the thermodynamic pressure is

$$p = c_s^2\rho + \frac{c_s^2 g}{2}\psi^2, \tag{27}$$

which can be determined from a nonideal-gas EOS. We can use the following strategy [3,22,23]:

$$\psi = \sqrt{\frac{2(p - c_s^2\rho)}{c_s^2 g}}, \tag{28}$$

to incorporate different EOSs into the SC LBM.

For interparticle-force model B, the corresponding pressure tensor can be derived similarly [20]. Here we propose using the following formula to incorporate different EOSs into the SC model:

$$\psi = \sqrt{\frac{2(p - c_s^2\rho)}{c_s^2(g_1 + 2g_2)}}. \tag{29}$$

A. Typical equations of state used in the simulations

Here we illustrate some popular equations of state which are subsequently investigated in the context of the SC model. The van der Waals (vdW) EOS is the simplest and most well-known cubic EOS [22]:

$$p = \frac{\rho RT}{1 - b\rho} - a\rho^2, \tag{30}$$

where $a = \frac{27(RT_c)^2}{64p_c}$, $b = \frac{RT_c}{8p_c}$, R is the gas constant, and T is the temperature. The Carnahan-Starling (CS) EOS is given by [22]

$$p = \rho RT\frac{1 + b\rho/4 + (b\rho/4)^2 - (b\rho/4)^3}{(1 - b\rho/4)^3} - a\rho^2, \tag{31}$$

with $a = 0.4963R^2T_c^2/p_c$ and $b = 0.18727RT_c/p_c$.

For the vdW EOS, we set $a = 9/49$, $b = 2/21$, $R = 1$, and the critical density $\rho_c = 3.5$. For the CS EOS, the parameters are $a = 1$, $b = 4$, $R = 1$ and $\rho_c = 0.1136$. In the following study, if not specified, usually the CS EOS is used because it allows one to achieve the highest density ratio [22].

B. Derivation of the analytical surface tension

The following derivation of the analytical surface tension in the SC LBM is identical to those described in Refs. [18,19]. We repeat the essential steps for the readers' convenience. In the following discussion, we assume that a flat interface parallel to the x-z plane separates liquid and gas. The phase interface implicitly defined by $\rho = (\rho_l + \rho_g)/2$ is chosen as the origin of the y axis. For interparticle-force model A, the normal component of the pressure tensor p_{yy} obtained from Eq. (26) is

$$p_{yy} = c_s^2\rho + \tfrac{1}{2}gc_s^2\psi^2 + \tfrac{1}{2}gc_s^4\left(\psi\partial_{yy}\psi - \tfrac{1}{2}\partial_y\psi\partial_y\psi\right). \tag{32}$$

In both phases far from the interface the pressure p_0 satisfies the following relation [18,19]:

$$p_0 = c_s^2\rho_g + \tfrac{1}{2}gc_s^2\psi^2(\rho_g) = c_s^2\rho_l + \tfrac{1}{2}gc_s^2\psi^2(\rho_l). \tag{33}$$

One obtains the density profile $d\rho/dy$ by solving Eqs. (32) and (33) assuming $d\rho/dy = 0$ at $y = \pm\infty$. A simple change of variables simplifies Eq. (32). In order to get a formal solution, we set $(d\rho/dy)^2 = z$ and notice that $\frac{d^2\rho}{dy^2} = \frac{1}{2}\frac{dz}{d\rho}$; then Eq. (32) can be transformed as follows [18,19]:

$$p_{yy} = c_s^2\rho + \frac{1}{2}gc_s^2\psi^2 + \frac{1}{4}gc_s^4\frac{\psi^2}{\psi'}\frac{d}{d\rho}\left(z\frac{\psi'^2}{\psi}\right), \tag{34}$$

where $\psi' = \partial\psi/\partial\rho$. By direct integration and using the definition of Eq. (27), one can obtain the following solution for $z(\rho)$ [18,19]:

$$\begin{aligned} z(\rho) &= \frac{4\psi}{gc_s^4(\psi'^2)}\int_{\rho_g}^{\rho}\left(p_{yy} - c_s^2\rho - \frac{1}{2}gc_s^2\psi^2\right)\frac{\psi'}{\psi^2}d\rho \\ &= \frac{4\psi}{gc_s^4(\psi'^2)}\left[\left(-\frac{p_0}{\psi} + \frac{p_{yy}}{\psi}\right)\Big|_{\rho_g}^{\rho} - \int_{\rho_g}^{\rho}\frac{dp_{yy}/d\rho}{\psi}d\rho\right]. \end{aligned} \tag{35}$$

To satisfy the boundary condition [i.e., Eq. (33)], we require

$$\int_{\rho_g}^{\rho_l}\left(p_{yy} - c_s^2\rho - \frac{1}{2}gc_s^2\psi^2\right)\frac{\psi'}{\psi^2}d\rho = 0. \tag{36}$$

The quantities p_0, ρ_l, and ρ_g can be simultaneously obtained numerically from Eq. (36). Then, by solving Eq. (35), the density profile in the vicinity of the interface can be obtained. Finally, the surface tension can be computed from [18,19]

$$\sigma = -\frac{1}{2}gc_s^4\int_{-\infty}^{+\infty}(\partial_y\psi)^2dy = -\frac{1}{2}gc_s^4\int_{-\infty}^{+\infty}\psi'^2[z(\rho)]^{1/2}d\rho. \tag{37}$$

For interparticle-force model B, one can obtain the pressure tensor by an analogous procedure. The result is similar to Eq. (26) [20]:

$$\begin{aligned} p^*_{\alpha\beta} = &\left[c_s^2\rho + \tfrac{1}{2}A_1c_s^2\psi^2 + \tfrac{1}{2}A_2c_s^4(\psi\Delta\psi + \tfrac{1}{2}|\nabla\psi|^2)\right]\delta_{\alpha\beta} \\ &- \tfrac{1}{2}A_2c_s^4\partial_\alpha\psi\partial_\beta\psi, \end{aligned} \tag{38}$$

where A_1 and A_2 are constants related to g_1 and g_2 in Eq. (23),

$$A_1 = g_1 + 2g_2, \quad A_2 = g_1 + 8g_2. \tag{39}$$

The corresponding surface tension is

$$\sigma^* = -\frac{1}{2}A_2c_s^4\int_{-\infty}^{+\infty}(\partial_y\psi)^2dy. \tag{40}$$

V. RESULTS AND DISCUSSION ON MULTIPHASE FLOWS

In this section we study the properties of the original SC model and the SC model in combination with the other four forcing strategies. All simulations in this section use interparticle-force model A, except for Sec. V G.

In our study, not only were the cases of a cylindrical droplet simulated, but also the cases of a flat interface. For the cases of a flat interface, the computational domain is $N_x \times N_y = 10 \times 200$, with periodic boundary conditions in both directions. The central region ($50 \leqslant y \leqslant 150$) and the other region were filled with liquid and gas, respectively. The density field was initialized as $\rho(y) = \rho_{\text{gas}} + \frac{\rho_{\text{liquid}} - \rho_{\text{gas}}}{2}[\tanh(\frac{2(y-50)}{W}) - \tanh(\frac{2(y-150)}{W})]$, where W is the initial interface thickness, which is always chosen as 5 l.u. in our simulations. The units of the density and the surface tension are m.u./l.u.^{3} and m.u./t.s.^{2}, respectively.

For the cylindrical droplet cases, if not specified, the computational domain consists of 200×200 grid nodes and a central circular area with liquid was initialized in the domain and the other part was initialized as a lower density area (gas). Periodic boundary conditions were applied in both directions.

The analytical densities at a specified temperature and zero velocity were used as initial conditions. The density field was initialized as

$$\rho(x,y) = \frac{\rho_{\text{liquid}} + \rho_{\text{gas}}}{2} - \frac{\rho_{\text{liquid}} - \rho_{\text{gas}}}{2} \times \left[\tanh\left(\frac{2(\sqrt{(x-x_1)^2+(y-y_1)^2} - R_0)}{W}\right)\right],$$

where (x_1, y_1) is the center position of the domain and R_0 is the initial radius of the droplet. The convergence criterion is

$$\frac{\sum |[u(t) - u(t-2000)]| + |[v(t) - v(t-2000)]|}{\sum |u(t)| + |v(t)|} < 10^{-7}$$

and the summation is taken over the whole computational domain. We checked that this criterion is sufficient to let the flat interface and the droplet reach the equilibrium state.

A. Spatial accuracy

The single-phase LBM is usually second-order accurate in space. One may be interested in the spatial accuracy of the LBM for multiphase flows. The spatial accuracy of the SC model combined with the five schemes is tested by the cases of a cylindrical droplet first. To test the accuracy, different mesh sizes $N_x \times N_y = 50 \times 50$, 100×100, 150×150, and 200×200 are used. The radius of the droplet is $R_0 = \frac{1}{4}N_x$. Here we assume that the mesh 200×200 is the finest mesh and the result at this mesh is accurate. The error of mesh size N_x is defined as $\text{Error}(N_x) = |\rho(N_x) - \rho(200)|$, where $\rho(N_x)$ means the density of liquid or gas obtained by mesh size $N_x \times N_x$. The errors of different schemes are illustrated in Fig. 2, where we can see that schemes I, III, and V are approximately second-order accurate in space. This conclusion is not relevant to the τ value. For example, errors of scheme I with $\tau = 0.7\Delta t$ and $1.0\Delta t$ exhibit almost the same spatial accuracy (the result of $\tau = 1.0\Delta t$ is not shown). Hence, here we confirm that the LBM for multiphase flow has approximately second-order spatial accuracy. Note that here the error of scheme IV is identical to that of scheme III. Scheme II is not evaluated here because it gives the wrong results in multiphase flow simulations, which will be illustrated in the following.

B. Droplet-size effect

In the following study, the effective surface tension of a numerical scheme is obtained from the simulation results of a droplet immersed in the gas, which can be described by the Laplace law. After the drop radius R_0 and the pressure difference inside p_{in} and outside p_{out} the drop are measured, the surface tension σ can be determined from $\frac{\sigma}{R_0} = p_{\text{in}} - p_{\text{out}}$, where R_0 is the distance between the center of the circle and a point where $\rho = (\rho_{\text{in}} + \rho_{\text{out}})/2$.

As the drop size may slightly affect the equilibrium density contrast and the surface tension in all multiphase LBMs with force strategy [17], we investigate these drop-size effects by simulating cases with different initial drop sizes. In the simulations, the original SC model (scheme I) is used and the other parameters are $\frac{T}{T_0} = 0.825$ and $\tau = \Delta t$. In the final equilibrium state, two cases with droplet radii of 19.3 and 59.3 l.u. result in density contrasts of 0.2949/0.024 88 and 0.2935/0.023 96 and the surface tensions are 5.747×10^{-3} and 5.916×10^{-3} m.u./t.s.^{2}, respectively. The relative density ratio and surface tension difference in the two cases are less than 3.3%.

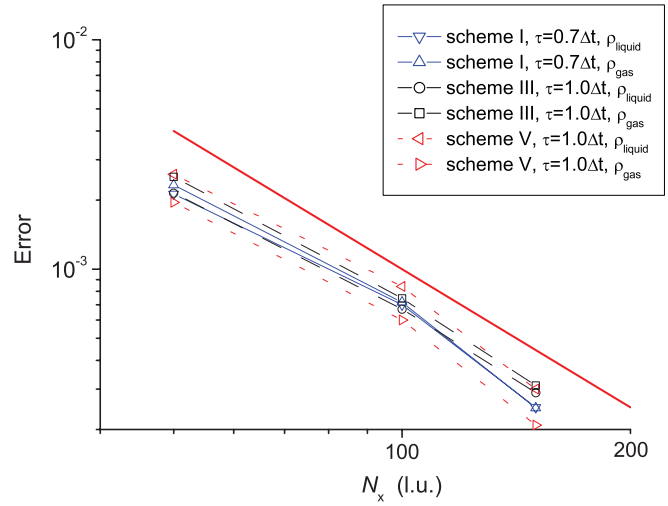

FIG. 2. (Color online) Error of the densities of liquid and gas as a function of mesh size. The slope of the top thick line is −2. The line represents the exact second-order spatial accuracy, which is used to guide the eyes. The other solid, dashed, and dotted lines correspond to schemes I, III, and V, respectively.

For the SC model with scheme III, to test the droplet-size effect, cases of $\frac{T}{T_0} = 0.825$ and $\tau = \Delta t$ were simulated. In the final equilibrium state, two cases with droplet radii of 16.2 and 35.4 l.u. result in density contrasts of 0.2920/0.016 67 and 0.2908/0.015 40 and the surface tensions are 3.397×10^{-3} and 3.506×10^{-3} m.u./t.s.^{2}, respectively. The relative density ratio and surface tension difference in the two cases are less than 3.1%. Hence we conclude that the drop-size effects are negligible for the problems under consideration.

For the SC model with other schemes, the drop-size effect is also found to be negligible. In the following simulations the drop radius is set as approximately 30 l.u.

C. Comparison between schemes in group B

We start by comparing schemes III and IV. In the preceding analysis, these schemes were proved to be the same when terms of $O(u^3)$ are neglected (group B). Here numerical tests are performed. A case of the CS EOS, with $\frac{T}{T_c} = 0.85$ and $\tau = 1.0\Delta t$, was simulated. The $|\mathbf{u}_{\max}|$ obtained by schemes III and IV are 0.001 402 12 and 0.001 402 11 l.u./t.s., respectively. The densities ρ_l/ρ_g are 0.277 143 747 3/0.022 913 706 6 and 0.277 143 747 5/0.022 913 706 5, respectively. The corresponding surface tensions are 0.002 671 921 and 0.000 267 192 2 m.u./t.s.^{2}, respectively. Here we can see that to an accuracy of 10^{-7}, the spurious currents, densities, and surface tensions of the two schemes are identical. For other cases with different τ and $\frac{T}{T_c}$, in terms of the spurious currents, densities, and surface tensions, numerical tests also confirmed that to $O(u^2)$, schemes III and IV are identical, which is consistent with our theoretical analysis. Hence, in the following study, only scheme III will be discussed.

TABLE II. Density ratios and surface tension obtained from the original SC model (scheme I) with $\tau/\Delta t = 0.6$.

$\frac{T}{T_c}$	Droplet ρ_l/ρ_g	σ ($\times 10^{-3}$)	Flat interface ρ_l/ρ_g	Analytical ρ_l/ρ_g	σ ($\times 10^{-3}$)
0.95	0.2099/0.06500	0.4892	0.2087/0.06366	0.2097/0.06553	0.5690
0.90	0.2464/0.04014	1.421	0.2454/0.03908	0.2471/0.04299	1.638
0.85	0.2770/0.02283	2.766	0.2759/0.02171	0.2781/0.02781	3.061
0.80	N/A	N/A	N/A	0.3060/0.01674	4.834

D. Comparison between schemes in group A

For schemes I (the original SC model), II, and V, the situation is different from the preceding. First we compare schemes I and V.

It is worth mentioning that for $\tau = \Delta t$, the results of schemes I and V are found to be identical (down to an accuracy of 10^{-15}) for the same parameter set, while for $\tau \neq \Delta t$ the results of the two schemes show significant deviations from each other. The τ effect will be discussed in Sec. V E.

The density ratios and surface tensions obtained from schemes I and V are shown in Tables II and III, respectively. Both densities in the cases of the cylindrical droplet and the flat interface are listed in the tables. Analytical solutions are also illustrated. In this paper, if not specified, the analytical solutions are obtained through the mechanical stability condition [19], which means that the densities ρ_l and ρ_g satisfy Eq. (36). In contrast, in the case of thermodynamic consistency, ρ_l and ρ_g can be obtained from the Maxwell equal-area construction in the p-v diagram of the EOS [which requires $\int_{v_l}^{v_g} (p_0 - p)dv = 0$, where $v = \frac{1}{\rho}$ and p_0 is a constant for a specific temperature]. From Eq. (36) we can see that only if $\psi(\rho) \propto \rho$, the SC model is thermodynamically consistent [19]. However, most EOSs do not satisfy this constraint. Hence the coexistence curves obtained from the mechanical stability condition and the thermodynamic equilibrium show small discrepancies.

From the tables we can see that the difference between densities obtained from cases of the cylindrical droplet and the flat interface is less than 5% and 7% in Table II and III, respectively. Hence the results obtained by simulations of the cylindrical droplet and the flat interface are very consistent.

For the densities of liquid and gas, Tables II and III show that the numerical results are consistent with the analytical ones at higher $\frac{T}{T_c}$. For decreasing temperatures, the difference between numerical and analytical ρ_g will increase. In Table II the maximum difference between the numerical (cases of a cylindrical droplet) and analytical ρ_g is approximately 28% at $\frac{T}{T_c} = 0.85$. In Table III the maximum difference is approximately 34% at $\frac{T}{T_c} = 0.75$.

This discrepancy between numerical and analytical ρ_g may be caused by the terms of $O(\frac{(\mathbf{F}\Delta t)^2}{\rho})$ in Eqs. (16) and (17). We also note that the coefficient before the terms of $O(\frac{(\mathbf{F}\Delta t)^2}{\rho})$ is different in schemes I and V. Hence the stability behavior and densities of liquid and gas of the two schemes are different. This also means that the terms of $O(\frac{(\mathbf{F}\Delta t)^2}{\rho})$ significantly affect the performance of schemes I and V.

For the surface tension, Table II shows that the numerical results of scheme I are more consistent with the analytical ones (the maximum difference at $\frac{T}{T_c} = 0.85$ is approximately 10%). Table III demonstrates that the surface tension obtained by scheme V at $\tau = 0.6\Delta t$ is significantly different from the analytical one for any $\frac{T}{T_c}$ (the maximum difference is approximately 50% compared with the analytical one).

Now scheme II is investigated in detail. The density ratios obtained by scheme II are found to be approximately consistent with the analytical results. However, it is unfortunate that the numerical surface tension is negative, which is entirely unphysical. The stability of this scheme is also found to be the worst among the five schemes. For example, the lowest temperature for $\tau = \Delta t$ is about $T = 0.925T_c$. That may due to the lack of terms of $O(\frac{(\mathbf{F}\Delta t)^2}{\rho})$ in scheme II compared to schemes I and V. Hence, although scheme II works well for single-phase flow, it does not seem so successful for multiphase flow. In the follows, we will no longer discuss scheme II.

E. τ effect

In this section the dependence of the surface tension and the density ratio on the relaxation time τ is discussed in detail. Comparisons are carried out for the original SC model (scheme I) and the SC model in combination with schemes III and V. The comparison focuses on the resulting surface tension issue, which is a very important property in the multiphase-flow simulations.

TABLE III. Density ratios and surface tension obtained from the SC model with scheme V for $\tau/\Delta t = 0.6$.

$\frac{T}{T_c}$	Droplet ρ_l/ρ_g	σ ($\times 10^{-3}$)	Flat interface ρ_l/ρ_g	Analytical ρ_l/ρ_g	σ ($\times 10^{-3}$)
0.95	0.2111/0.06692	0.8622	0.2099/0.06583	0.2097/0.06553	0.5690
0.90	0.2487/0.04474	2.550	0.2475/0.04380	0.2471/0.04299	1.638
0.85	0.2799/0.03002	4.713	0.2786/0.02912	0.2781/0.02781	3.061
0.80	0.3074/0.01909	7.267	0.3065/0.01854	0.3060/0.01674	4.834
0.75	0.3343/0.01163	10.251	0.3326/0.01085	0.3321/0.008632	6.932
0.70	N/A	N/A	N/A	0.3572/0.003120	9.386

TABLE IV. Density ratios and surface tension obtained from the SC model with scheme III for $\frac{T}{T_c} = 0.825$. (The analytical densities and surface tension are $\rho_l/\rho_g = 0.2923/0.021\,85$ and $\sigma = 3.912 \times 10^{-3}$ m.u./t.s.^{2} for any τ.)

$\tau/\Delta t$	Droplet ρ_l/ρ_g	σ ($\times 10^{-3}$)	$\lvert\mathbf{u}\rvert_{\max}$	Flat interface ρ_l/ρ_g
0.60	0.2909/0.01530	3.543	0.01095	N/A
0.65	0.2909/0.01531	3.541	0.006060	N/A
0.70	0.2908/0.01520	3.579	0.003861	0.2898/0.01429
0.80	0.2908/0.01525	3.581	0.001681	0.2898/0.01429
0.90	0.2907/0.01517	3.486	0.002013	0.2898/0.01429
1.00	0.2908/0.01538	3.591	0.002183	0.2898/0.01429
2.00	0.2911/0.01606	3.638	0.004479	0.2898/0.01429

TABLE V. Density ratios and surface tension obtained from the original SC model (scheme I) for $\frac{T}{T_c} = 0.825$. (The analytical densities and surface tension are $\rho_l/\rho_g = 0.2923/0.021\,85$ and $\sigma = 3.912 \times 10^{-3}$ m.u./t.s.^{2} for any τ.)

$\tau/\Delta t$	Droplet ρ_l/ρ_g	σ ($\times 10^{-3}$)	$\lvert\mathbf{u}\rvert_{\max}$	Flat interface ρ_l/ρ_g
0.60	N/A	N/A	N/A	0.2900/0.01468
0.65	0.2912/0.01618	3.693	0.005474	0.2901/0.01516
0.70	0.2915/0.01687	3.993	0.002918	0.2904/0.01584
0.80	0.2923/0.01880	4.338	0.001671	0.2910/0.01773
0.90	0.2933/0.02140	4.998	0.001965	0.2919/0.02029
1.00	0.2939/0.02418	5.807	0.002230	0.2928/0.02342
2.00	0.3003/0.05922	15.31	0.01049	0.2977/0.05391

Table IV illustrates the equilibrium densities of liquid ρ_l and gas ρ_g and the resulting surface tension obtained from scheme III for $\frac{T}{T_c} = 0.825$. For the cases of a cylindrical droplet in Table IV, when τ changes from $0.6\Delta t$ to $1.0\Delta t$, the variation in ρ_g and surface tension σ variation are less than 1.4% and 3.0%, respectively. Hence, in terms of the density ratio and surface tension, the SC model in combination with scheme III is not sensitive to the variation of τ. The cases of a flat interface also demonstrate that the densities do not change with τ, although simulations of a flat interface seems slightly less stable than those of a cylindrical droplet.

To further investigate forcing scheme III, we simulate cases for different temperatures and τ. Figure 3 illustrates the surface tension, densities of liquid and gas, and density ratio as a function of $\frac{T}{T_c}$. Figures 3(a), 3(b), and 3(c) demonstrate that ρ_{liquid}, ρ_{gas}, and σ, respectively, do not change with τ for a given temperature. The numerical ρ_{gas} agrees better with the analytical solution obtained from the mechanical stability condition than that from thermodynamic coexistence. Because the numerical ρ_{gas} is slightly smaller than the analytical ρ_{gas}, the density ratio of liquid and gas is significantly larger than the analytical one [Fig. 3(d)]. The small discrepancy between the analytical and numerical ρ_{gas} may be caused by the compressibility in the SC model or the effect of spurious currents and require further investigation. In Fig. 3(c) the constant surface tensions obtained for $\tau = 0.6\Delta t, 0.8\Delta t$, and $1.0\Delta t$ all agree well with the theoretical σ, which is obtained by the mechanical stability condition.

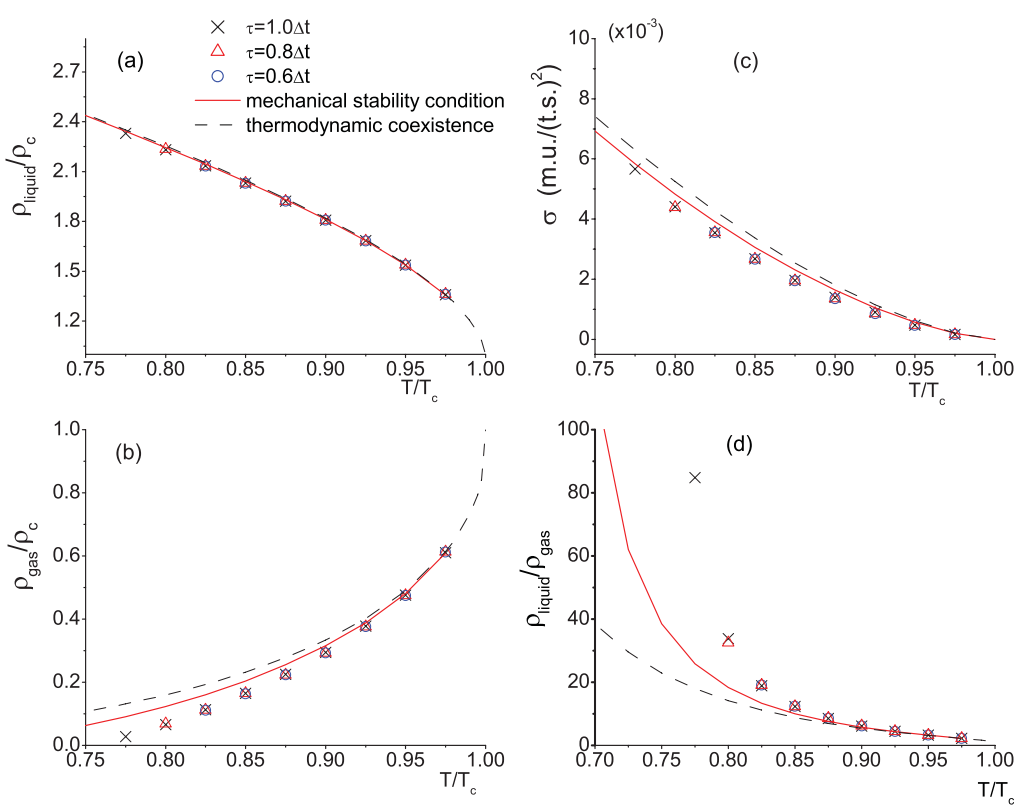

FIG. 3. (Color online) Results obtained by the SC model with the CS EOS and forcing scheme III for different values of τ: (a) reduced density of liquid, (b) reduced density of gas, (c) surface tension, and (d) liquid-to-gas density ratio as a function of T/T_c.

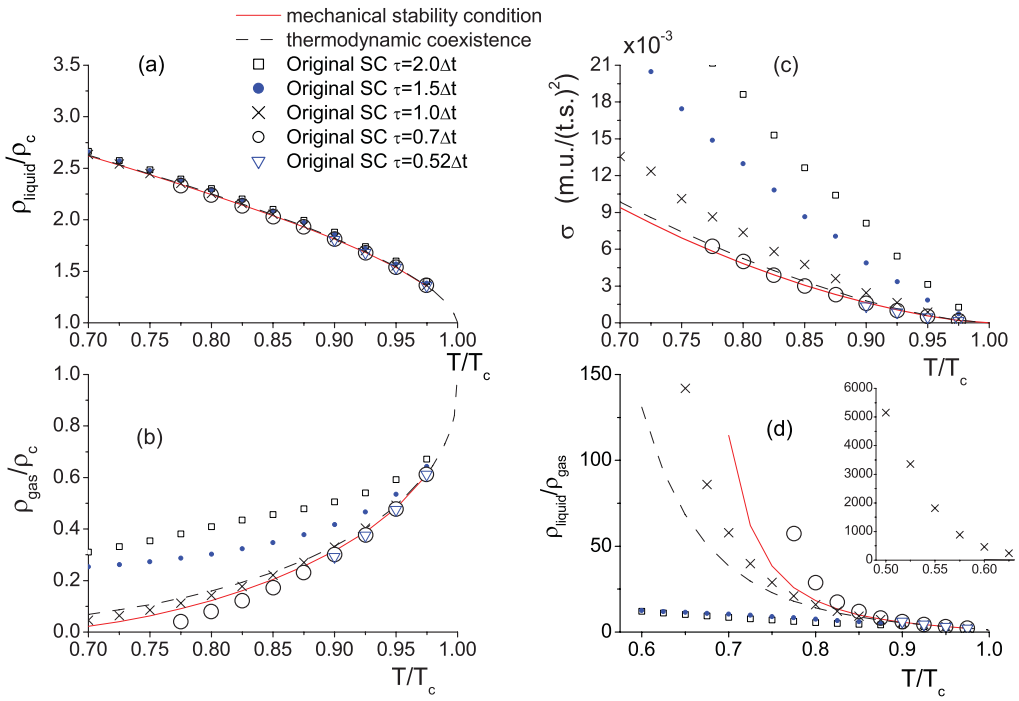

FIG. 4. (Color online) Results obtained by the original SC model (scheme I) for different values of τ: (a) reduced density of liquid, (b) reduced density of gas, (c) surface tension, and (d) liquid-to-gas density ratio as a function of T/T_c for the CS EOS.

For the original SC model (scheme I), Table V shows that changing τ from $0.65\Delta t$ to $2.0\Delta t$ leads to an increase of ρ_g and surface tensions of 265% and 314%, respectively. The τ effect is very strong in scheme I.

For scheme I, Fig. 4 illustrates $\rho_{\text{liquid}}, \rho_{\text{gas}}, \sigma$, and the density ratio as a function of $\frac{T}{T_c}$. In Fig. 4(c) the surface tensions obtained from $\tau = 0.7\Delta t$, $0.55\Delta t$, and $0.52\Delta t$ are consistent with the analytical values, while those values obtained from cases of $\tau = 1.0\Delta t$, $1.5\Delta t$, and $2\Delta t$ are much larger than the analytical one. Hence the surface tension calculated from the original SC model depends on the value of τ, which is unphysical.

In Fig. 4(b) the ρ_{gas} obtained from $0.52\Delta t < \tau < \Delta t$ seems more consistent with the analytical solution than $\tau = 1.5\Delta t$ and $2.0\Delta t$. When $\tau = 1.5\Delta t$ and $2.0\Delta t$, the numerical ρ_{gas} is significantly different from the analytical ρ_{gas} and the density ratio of liquid to gas severely deviates from the analytical ones [Fig. 4(d)]. From Fig. 4(d) it is found that when $\tau \approx \Delta t$ (crosses), the simulation remains very stable even at $\frac{T}{T_c} = 0.5$. The maximum density ratio that this scheme can achieve is about 5000 when $\tau = \Delta t$.

TABLE VI. Density ratios and surface tension obtained from the SC model with scheme V for $\frac{T}{T_c} = 0.825$. (The analytical densities and surface tension are $\rho_l/\rho_g = 0.2923/0.021\,85$ and $\sigma = 3.912 \times 10^{-3}$ m.u./t.s.^{2} for any τ.)

$\tau/\Delta t$	Droplet ρ_l/ρ_g	σ ($\times 10^{-3}$)	$\lvert\mathbf{u}\rvert_{\max}$	Flat interface ρ_l/ρ_g
0.60	0.2794/0.02967	4.662	0.002334	0.2928/0.02342
0.65	0.2794/0.02968	4.663	0.001253	0.2928/0.02342
0.70	0.2794/0.02968	4.665	0.000947	0.2928/0.02342
0.80	0.2794/0.02971	4.670	0.001190	0.2928/0.02342
0.90	0.2794/0.02974	4.677	0.001381	0.2928/0.02342
1.00	0.2794/0.02977	4.686	0.002112	0.2928/0.02342
2.00	0.2795/0.02996	4.774	0.002449	0.2928/0.02342

Finally, we discuss scheme V. Table VI demonstrates that for the cases of a cylindrical droplet, a different τ has only a negligible effect on the densities and surface tension at $T = 0.825T_c$. For the cases of a flat interface, the densities of liquid and gas are not affected by τ at all. Hence, at $T = 0.825T_c$, the result is almost independent of τ.

Figure 5 illustrates the reduced density of the liquid and gas, the surface tension, and the density ratio as a function of T/T_c. At a specific temperature, the ρ_{gas} that is obtained from different τ seem almost identical. However, from Fig. 5(d) we can see that at lower temperatures, for example, $\frac{T}{T_c} < 0.65$, the density ratio is still affected by τ significantly. From Fig. 5(c) we can see that the surface tensions obtained from different τ are highly consistent. However, they all deviate from the analytical one.

As a minor conclusion, scheme III is independent of τ. The numerical results (the density of the gas and the surface tension) of scheme I strongly depend on τ. For scheme V the surface tension is almost unaffected by τ, but the values deviate from the analytical ones. The density ratio obtained from scheme V is slightly affected by τ.

The conclusion about the τ effect is applicable not only to the CS EOS but also to the other EOS. As an example, cases of a cylindrical droplet using the vdW EOS were also simulated. The surface tensions obtained from the original SC model (scheme I) and the SC model in combination with scheme III are shown in Fig. 6. Again, we can see that the numerical surface tensions of schemes III and I with $\tau = 0.6\Delta t$ agree

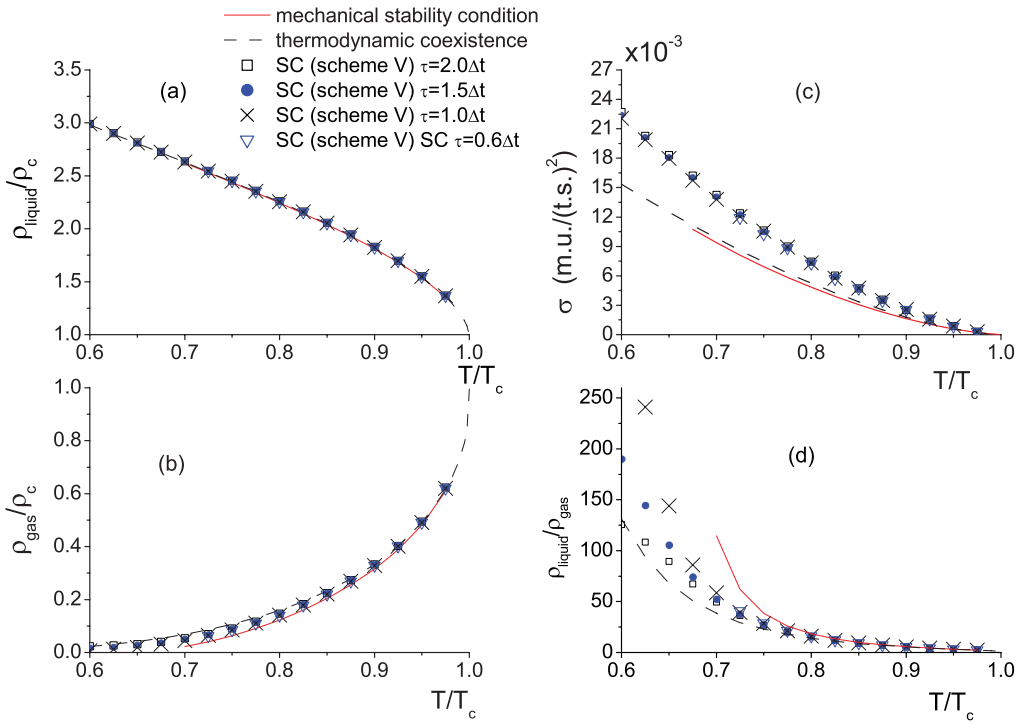

FIG. 5. (Color online) Results obtained by the SC model in combination with scheme V for different values of τ: (a) reduced density of liquid, (b) reduced density of gas, (c) surface tension, and (d) density ratio as a function of T/T_c for the CS EOS.

well with the analytical solutions. However, when $\tau = \Delta t$ and $1.5\Delta t$, there are large discrepancies between the results of scheme I and the analytical solutions.

F. Stability

In this section we discuss numerical stability for multiphase flow simulations. The numerical stability depends on the forcing schemes. For example, when using the original SC model (scheme I) with $\tau = \Delta t$, the simulation remains stable even at $\frac{T}{T_c} = 0.50$ [corresponding to an equilibrium density ratio of 5000; refer to Fig. 4(d)]. The maximum density ratio of the SC model with scheme III is limited to $0.3175/0.003\,748 = 84.78$ at $\frac{T}{T_c} = 0.775$ [refer to Fig. 3(d)]. For scheme V the maximum density ratio is limited to $0.4195/0.000\,467\,7 = 896.94$ at $\frac{T}{T_c} = 0.575$. This means that the numerical stability of the original SC model is substantially larger than that of forcing schemes III and V when $\tau = \Delta t$. Thus, in flow simulations where the maximum density ratio is of primary concern, the original SC model may be a good choice.

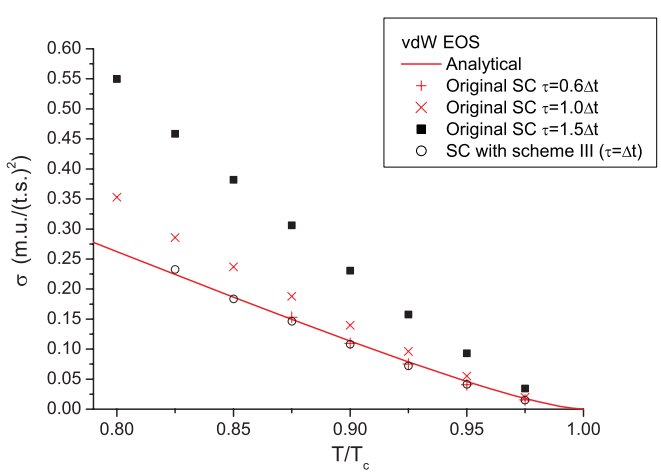

FIG. 6. (Color online) Surface tension σ as a function of T/T_c for the vdW EOS.

For different τ, the minimum $\frac{T}{T_c}$ that schemes I, III, and V can simulate are shown in Fig. 7. The upper right region of each line corresponds to the stable region of each scheme. Generally speaking, the numerical stability of scheme III is not as good as that of schemes I and V. The numerical stability depends on schemes partially because the schemes recover different macroequations. Although schemes I and V have better numerical stability for two-phase flow, they do not recover NS equations exactly. The extra terms in the momentum equation (compared to NS equations) may help stabilize schemes I and V.

It is found when the numerical instability appears, the interface usually only occupies 2 or 3 l.u. Since the SC multiphase model is a diffuse-interface method, the interface thickness is an important factor in simulations. Usually the thicker the interface is, the more stable the simulation would be. However, a very thick interface is not a good choice in multiphase flow simulations.

In the SC multiphase model, the interface is automatically formed and we are not able to adjust the interface thickness explicitly. The interface thickness depends on not only the temperature and τ, but also the formula of the EOS. The parameters a, R, and b in the CS EOS may affect the interface thickness and numerical stability. The present choice

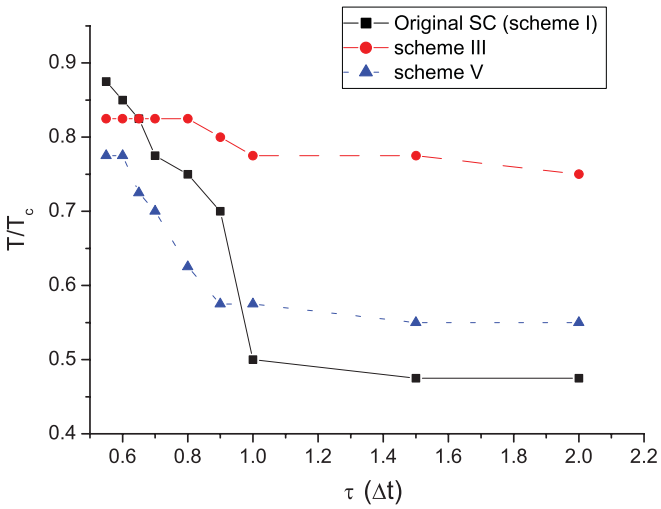

FIG. 7. (Color online) Stability of forcing schemes I, III, and V as a function of τ. The upper right region of each line is the corresponding stable region of each scheme. The CS EOS is used with $a = 1$, $R = 1$, and $b = 4$.

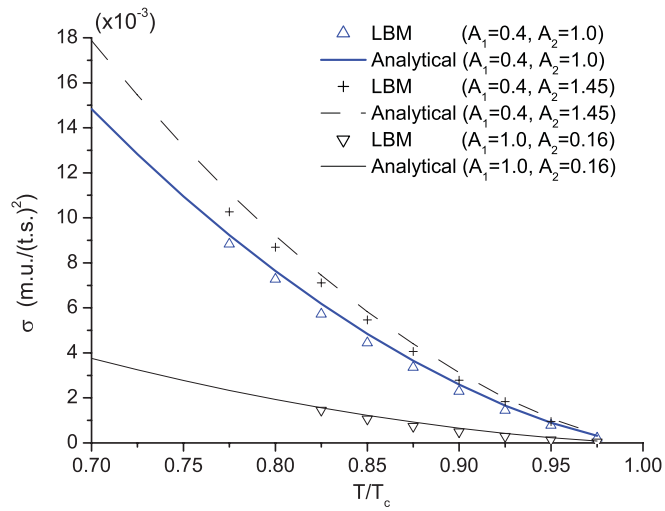

FIG. 8. (Color online) Surface-tension comparison between the SC model with forcing scheme III and the analytical solution for different A_1 and A_2. In the simulation, the interparticle force including next-nearest neighbors for the CS EOS is used and $\tau = \Delta t$.

of $a = 1$, $R = 1$, and $b = 4$ is appropriate because the interface thickness is approximate 5 l.u. for most T and τ.

To study the parameter effect, first $R = 1$ and $b = 4$ are fixed and the parameter a is allowed to change. We find that the interface widths are approximately 2, 3, 5, 7, and 11 l.u. for $a = 4$, 2, 1, 0.5, and 0.2, respectively, for a case of $\frac{T}{T_c} = 0.85$ and $\tau = 0.6\Delta t$ using scheme III. It seems that a large a leads to a thick interface.

To study the effect of b, $a = 1$ and $R = 1$ are fixed in simulations. The densities of the liquid and gas are affected by the parameter b, but the density ratio of liquid to gas would not change. We simulated a case of $\frac{T}{T_c} = 0.85$ and $\tau = 0.6\Delta t$ using scheme III. When $b = 0.5$, the simulation is not applicable. When $b = 1.0$ the interface is very sharp, the width of the interface is about 3 l.u. When $b = 20$, the interface occupies approximately 10 l.u., which is very thick. Through comparison, we know that $b = 1$ is a proper choice.

If we change only the gas constant R and fix the value of $a = 1$ and $b = 4$, the density ratio, surface tension, and thickness would not change with R. This is explained in the following. We note that Eq. (31) can be rewritten as

$$p = \frac{1.5092a}{b^2}\left\{\theta\left(\frac{T}{T_c}\right)\left[1 + \frac{-2\theta^2 + 4\theta}{(1-\theta)^3}\right] - 10.601\theta^2\right\}, \tag{41}$$

where $\theta = \frac{b}{4}\rho$. In the above derivation, the relationship between the critical temperature and the parameters $T_c = \frac{0.3773a}{bR}$ for the CS EOS is used. Obviously the parameter R will not affect the phase-separation property at a specific $\frac{T}{T_c}$. Overall, after the parameters in the EOS are properly chosen, forcing schemes would affect the numerical stability significantly when the SC model is used.

G. Interparticle-force model B

We also carry out simulations using the interparticle-force model B [20]. These results are compared with the analytical result obtained from Eq. (40). Behaviors similar to those in Figs. 3 and 4 are observed, i.e., the SC model in combination with scheme III and the original SC model (for $\tau < 0.7\Delta t$) are consistent with the analytical solutions. Figure 8 shows the surface tension obtained from the SC model in combination with scheme III. The numerical results agree well with the analytical ones for different combination of A_1 and A_2.

In Ref. [8] an approximation for the interparticle force is proposed as

$$\mathbf{F}_{\text{int}}(\mathbf{x},t) = -g\left[(1-2A)\psi(\mathbf{x},t)\sum_i w_i\psi(\mathbf{x}+\mathbf{e}_i\Delta t,t)\mathbf{e}_i + A\sum_i w_i\psi^2(\mathbf{x}+\mathbf{e}_i\Delta t,t)\mathbf{e}_i\right], \tag{42}$$

which slightly differs from the one proposed by Sbragaglia *et al.* [20] [i.e., Eq. (23)], but actually the idea is similar. A Taylor expansion of Eq. (42) results in

$$F_\alpha(\mathbf{x},t) \approx -\frac{g}{2}\Delta t c_s^2\partial_\alpha\psi^2 - \frac{g}{2}\Delta t^3 c_s^4\psi(\partial_\alpha\nabla^2\psi) - \left\{gA\Delta t^3 c_s^4(\partial_\alpha\psi\nabla^2\psi + 2\partial_\beta\psi\partial_\alpha\partial_\beta\psi)\right\}. \tag{43}$$

TABLE VII. Density ratio for different surface tensions (the SC model with forcing scheme III for $\tau = \Delta t$ and the CS EOS).

$\frac{T}{T_c}$	$\sqrt{\frac{A_2}{A_1}}$	ρ_l/ρ_g	σ ($\times 10^{-3}$)
0.85	1.0	0.2768/0.02250	2.683
0.85	1.458	0.2785/0.02587	4.199
0.85	1.904	0.2795/0.02775	5.461
0.775	1.0	0.3175/0.003745	5.661
0.775	1.458	0.3191/0.008159	7.939
0.775	1.904	0.3201/0.01052	10.57

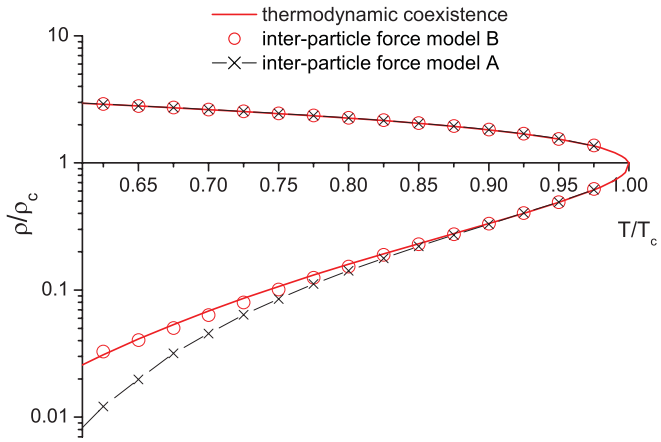

FIG. 9. (Color online) Coexistence curve for the CS EOS: The solid line is the analytical solution obtained from the Maxwell construction (corresponding to thermodynamic consistency). The numerical results were obtained by the original SC model with $\tau = \Delta t$.

Thus the difference between Eqs. (43) and (24) lies in the terms inside the curly braces in Eq. (43). The surface tension can be changed by modifying the parameter A.

In Ref. [20] Sbragaglia *et al.* argue that the surface tension can be changed without affecting the density ratio. However, in our study, we find that the density ratio changes when modifying the ratio of $\frac{A_2}{A_1}$. An example for the SC model with forcing scheme III with $\tau = \Delta t$ and the CS EOS is illustrated in Table VII. From the table we can see that for a relatively large ratio $\frac{T}{T_c} = 0.85$ the density ratio changes are small, yet for $\frac{T}{T_c} = 0.775$ they are more pronounced.

If the deviation of the surface tension from the analytical solution and the density ratio dependence from τ is ignored, one can adjust the surface tension to force the densities to satisfy the thermodynamic coexistence condition, which essentially corresponds to mimicking thermodynamic consistency for the SC model. For the original SC model this adjustment is relatively easy: Fig. 9 shows the coexistence curve for the CS EOS. The numerical results are obtained for the original SC model with $\tau = \Delta t$. The result for interparticle-force model A shows a large discrepancy from the thermodynamic coexistence condition. However, using interparticle-force model B, we can adjust the densities to match the thermodynamic coexistence well by modifying the parameters of A_1 and A_2. In this simulation, $A_1 = 1.0$, $A_2 = 0.16$, $g_1 = 1.28$, and $g_2 = -0.14$. The relationship that these parameters should satisfy is illustrated in Eq. (39). The proper parameters were chosen through trial and error.

VI. CONCLUSION

Our theoretical analysis identified the relations between forcing schemes proposed by Shan and Chen [1] (scheme I), Luo [7] (scheme II), He *et al.* [9] (scheme III), Ladd and Verberg [10], Guo *et al.* [5] (scheme IV), and Kupershtokh *et al.* [8] (scheme V). We demonstrated that schemes I, II, and V are identical when terms of $O(\frac{F_\alpha F_\beta \Delta t^2}{\rho})$ in schemes I and V are omitted. Schemes III and IV are identical if terms of $O(u^3)$ in scheme III are neglected. Our numerical test of a classical unsteady flow problem confirmed that all schemes show the same convergence order for the single-phase flow problem.

For the multiphase flow simulations, the situation is different. In our study, the cases of a cylindrical droplet and a flat interface were simulated. A comparison of numerical results with the analytical solutions for a typical EOS, the surface tension obtained from the SC model using forcing scheme III (group B), is consistent and essentially independent from the value of τ. However, scheme II (group A) is unsuccessful simulating two-phase flow. For the original SC model (scheme I in group A), the density ratio and surface tension depend on the specific value of τ and large discrepancies between the numerical and analytical surface tensions were observed for $\tau > 0.7\Delta t$. For scheme V (group A), the density ratio is slightly affected by τ and the surface tension is almost τ independent, although the value deviates from the analytical one.

Although the SC model has been proven to be thermodynamically inconsistent, it is possible to restore thermodynamic consistency by adjusting the strength of the surface tension in order to match the coexistence curve obtained by the Maxwell construction. The forcing scheme of He *et al.* [9] (scheme III) for the SC model is found to be more accurate than schemes I, II, and V in terms of surface tension. To $O(u^2)$, schemes III and IV are identical. For the numerical stability in two-phase-flow simulations, scheme III is less stable than schemes I and V. These results may be useful for further study of two-phase flow with high density ratios based on the Shan-Chen LBM.

ACKNOWLEDGMENT

H.H. gratefully acknowledges financial support from the Alexander von Humboldt Foundation, Germany.

[1] X. Shan and H. Chen, Phys. Rev. E **47**, 1815 (1993).
[2] N. S. Martys and H. D. Chen, Phys. Rev. E **53**, 743 (1996).
[3] K. Sankaranarayanan, X. Shan, I. G. Kevrekidis, and S. Sundaresan, J. Fluid Mech. **452**, 61 (2002).
[4] T. Lee and C. L. Lin, J. Comput. Phys. **206**, 16 (2005).
[5] Z. Guo, C. Zheng, and B. Shi, Phys. Rev. E **65**, 046308 (2002).
[6] J. M. Buick and C. A. Greated, Phys. Rev. E **61**, 5307 (2000).
[7] L. S. Luo, Phys. Rev. Lett. **81**, 1618 (1998).
[8] A. L. Kupershtokh, D. A. Medvedev, and D. I. Karpov, Comput. Math. Appl. **58**, 965 (2009).
[9] X. He, X. Shan, and G. D. Doolen, Phys. Rev. E **57**, R13 (1998).
[10] A. J. C. Ladd and R. Verberg, J. Stat. Phys. **104**, 1191 (2001).
[11] A. K. Gunstensen, D. H. Rothman, S. Zaleski, and G. Zanetti, Phys. Rev. A **43**, 4320 (1991).
[12] D. H. Rothman and J. M. Keller, J. Stat. Phys. **52**, 1119 (1988).

[13] J. Tölke, S. Freudiger, and M. Krafczyk, Comput. Fluids **35**, 820 (2006).
[14] M. R. Swift, W. R. Osborn, and J. M. Yeomans, Phys. Rev. Lett. **75**, 830 (1995).
[15] X. Y. He, S. Y. Chen, and R. Y. Zhang, J. Comput. Phys. **152**, 642 (1999).
[16] A. J. Wagner, Phys. Rev. E **74**, 056703 (2006).
[17] E. S. Kikkinides, A. G. Yiotis, M. E. Kainourgiakis, and A. K. Stubos, Phys. Rev. E **78**, 036702 (2008).
[18] X. Shan and H. Chen, Phys. Rev. E **49**, 2941 (1994).
[19] R. Benzi, L. Biferale, M. Sbragaglia, S. Succi, and F. Toschi, Phys. Rev. E **74**, 021509 (2006).
[20] M. Sbragaglia, R. Benzi, L. Biferale, S. Succi, K. Sugiyama, and F. Toschi, Phys. Rev. E **75**, 026702 (2007).
[21] Z. Yu and L.-S. Fan, Phys. Rev. E **82**, 046708 (2010).
[22] P. Yuan and L. Schaefer, Phys. Fluids **18**, 042101 (2006).
[23] X. Y. He and G. D. Doolen, J. Stat. Phys. **107**, 309 (2002).
[24] M. Junk, A. Klar, and L. S. Luo, J. Comput. Phys. **210**, 676 (2005).
[25] X. W. Shan, X. F. Yuan, and H. D. Chen, J. Fluid Mech. **550**, 413 (2006).
[26] M. Gross, N. Moradi, G. Zikos, and F. Varnik, Phys. Rev. E **83**, 017701 (2011).